

# Achieving Spatial Scalability for Coded Caching over Wireless Networks

Mozhgan Bayat, Ratheesh K. Mungara, and Giuseppe Caire

## Abstract

The coded caching scheme proposed by Maddah-Ali and Niesen considers the delivery of files in a given content library to users through a deterministic error-free network where a common multicast message is sent to all users at a fixed rate, independent of the number of users. In order to apply this paradigm to a wireless network, it is important to make sure that the common multicast rate does not vanish as the number of users increases. This paper focuses on a variant of coded caching successively proposed for the so-called *combination network*, where the multicast message is further encoded by a *Maximum Distance Separable* (MDS) code and the MDS-coded blocks are simultaneously transmitted from different *Edge Nodes* (ENs) (e.g., base stations or access points). Each user is equipped with multiple antennas and can select to decode a desired number of EN transmissions, while either nulling or treating as noise the others, depending on their strength. The system is reminiscent of the so-called *evolved Multimedia Broadcast Multicast Service* (eMBMS), in the sense that the fundamental underlying transmission mechanism is multipoint multicasting, where each user can independently and individually (in a user-centric manner) decide which EN to decode, without any explicit association of users to ENs. We study the performance of the proposed system when users and ENs are distributed according to homogeneous Poisson Point Processes in the plane and the propagation is affected by Rayleigh fading and distance dependent pathloss. Our analysis allows the system optimization with respect to the MDS coding rate. Also, we show that the proposed system is fully scalable, in the sense that it can support an arbitrarily large number of users, while maintaining a non-vanishing per-user delivery rate.

## Index Terms

Coded Caching, Combination Network, Multipoint Multicasting, Stochastic Geometry.

The authors are with the Communications and Information Theory Group, Technische Universität Berlin, 10623 Berlin, Germany. E-mails: {bayat, mungara, caire}@tu-berlin.de.

## I. INTRODUCTION

With the forthcoming explosion of data traffic generated by the wireless Internet, it is important to consider schemes that take advantage of the user data consumption patterns. In particular, multimedia on-demand content delivery (especially video) is by far the most bandwidth consuming and rapidly growing application. Users typically make requests from some pre-existing video database/server (e.g., Netflix, YouTube, Hulu, Amazon Prime). This means that the user requests are highly redundant. In LTE, the *evolved Multimedia Broadcast Multicast Service* (eMBMS) standard was designed to simultaneously multicast popular common contents (e.g., live TV channels) to users in a wide area, by exploiting simultaneous transmission from multiple base stations. On the other hand, in the case of on-demand content delivery, the strongly asynchronous request patterns prevent from simply taking advantage of the broadcast nature of the wireless medium and transmit the same few files to a very large number of users. In order to take advantage of such *asynchronous content reuse*, wireless edge caching has been widely advocated in several different contexts (see for example the seminal work in [1, 2] and the stream of more recent works as in [3–6]).

In this work, we focus in particular on the elegant and information-theoretic near-optimal scheme known as *coded caching*, introduced by Maddah-Ali and Niesen in [7, 8]. The scheme was originally proposed for an idealized *single bottleneck network*, where a server is connected to  $K$  users through a shared error-free link of given capacity. The scheme of [7, 8] is based on two distinct phases: cache placement (or pre-fetching) and coded delivery. In the pre-fetching phase, to be performed before the network run time (e.g., in off-peak hours), the users cache segments of the library files either in a specified manner (centralized scheme [7]) or at random (decentralized scheme [8]). Then, during the network runtime, users make requests and the server responds with the transmission of a multicast coded message, computed such that each user can retrieve its requested file from the common multicast message and its own cache content. For the single bottleneck link network, the coded caching scheme (with an improved delivery that takes into account possibly repeated multiple requests) has been shown to be strictly optimal over all schemes with uncoded pre-fetching, i.e., when the users can cache segments of the library files and not general functions thereof [9]. In the recent work [10], general network topologies are considered and it is shown that the caching and delivery scheme of [7, 9], designed independently

of the underlying network, yields optimal performance within a bounded gap on any network, thus assessing a sort of “separation theorem” between caching and delivery.

Based on the coded caching idea, several other network topologies have been studied. A particularly relevant topology for the present paper is the so-called *combination network*, formed by the server, a layer of  $N_E$  intermediate nodes acting as relays, and the users. There are exactly  $K = \binom{N_E}{L}$  users, each of which is connected to a distinct subset of  $L$  out of  $N_E$  relays (from which the name “combination” network) [11–15]. Both the single bottleneck link network and the combination network are deterministic error-free models. On the other hand, in order to apply such caching paradigms to an actual wireless network, it is important to ensure that the content delivery rate does not vanish as the number of users become large. This represents a challenge in the presence of small-scale fading and distance dependent pathloss. We call *scalable* a scheme achieving a per-user delivery rate that tends to a positive limit as  $K \rightarrow \infty$ . In particular, for networks with constant user spatial density (users per unit area),  $K \rightarrow \infty$  implies that the network coverage area must grow linearly with  $K$ . In this case, a scalable scheme shall be referred to as *spatially scalable*, since the scheme can provide a fixed positive delivery rate for an arbitrarily large coverage area.

The goal of this work is to propose and analyze a spatially scalable scheme for on-demand content delivery based on coded caching. We consider a scenario motivated by eMBMS, where the content server is connected through high-capacity backhaul links to  $N_E$  wireless transmitters (e.g., base stations, access points, or remote radio heads), here referred to as *Edge Nodes* (EN) [5]. We argue that the combination network forms a good paradigm for a more general wireless network where any user can choose to receive data from  $L$  ENs in a completely autonomous user-centric way. In fact, since the combination network must serve all possible “user types” for all possible  $\binom{N_E}{L}$  connections, it follows that the users can roam free over the coverage area, and receive data as long as they can decode the messages of any subset of  $L$  ENs [11].

In coded caching, the common coded multicast message must be delivered to all users at a common rate, such that the system bottleneck is given by the worst-case user. It is well-known that such common broadcast rate vanishes in the presence of independent Rayleigh fading across the users  $K \rightarrow \infty$ . In [16] it is shown that transmitting with a multiantenna base station with growing number of antennas at least as  $\log K$  yields a scalable system. Nevertheless, such a single base station multi-antenna approach will not be effective against the pathloss, since all

antennas are concentrated at the base station site. Therefore, the approach of [16] is not spatially scalable. In contrast, in the proposed system, we consider spatially distributed single-antenna ENs, and users equipped with multiple antennas.<sup>1</sup> Using stochastic geometry, we show that the proposed system yields spatially scalable per user throughput in the presence of both small-scale Rayleigh fading and distance dependent pathloss. In addition, the proposed system is extremely simple, since no coordination among users and between the users and the ENs is required, and no joint signal space precoding across the ENs is used.

In current wireless technology, techniques that make use of spatially distributed antennas with various degrees of joint processing at the signal level are generally referred to as *Cloud radio access network* (C-RAN). In these schemes, ENs are connected to a centralized cloud processor. In full joint-processing C-RAN architectures, the cloud processor implements the baseband processing functionalities, including multiuser MIMO precoding [17–19]. In the context of caching, *Fog Radio Access Networks* (F-RANs) take a mixed approach between the C-RAN paradigm and *edge processing*, by equipping the ENs with caching capabilities [20–22]. In contrast to such cache-aided F-RAN systems, we consider that caching is performed in the user devices and, as already said, we assume that the backhaul links do not represent the system bottleneck, which is typically the case in eMBMS applications. Furthermore, in our scheme no joint baseband processing of the ENs is required. In fact, each EN simply broadcasts a network-coded message at fixed rate, without need of *transmitter channel state information*.

## II. SYSTEM MODEL

We consider a wireless network with  $N_E$  single-antenna ENs and  $K$  users, each equipped with an  $n_r$ -antenna array. A server is connected to the ENs via an error-free backhaul data network, of very high capacity. The system bottleneck is, realistically, the wireless segment between the ENs and the users. The server has access to a content library with  $N$  files represented by  $\mathcal{F} = \{W_1, W_2, \dots, W_N\}$ , each of which has a size of  $F$  bits. Each user has a cache memory of

<sup>1</sup>Typical hand-held devices operating at conventional cellular and WiFi frequency bands cannot host a large number of antenna elements. Nevertheless, for a relevant scenario we may think of a vehicular network where users are cars, which can host relatively large arrays, or a mmWave network, where a large number of antenna elements can be accommodated in a small form factor even on hand-held devices.

capacity  $MF$  bits. Since the backhaul network has very high capacity, the ENs do not need cache memory since whatever they have to transmit can be provided to them by the server. Following the paradigm of coded caching, we consider the pre-fetching phase and the delivery phase. The pre-fetching phase is identical to the optimal centralized strategy for the single bottleneck link network. This is recalled here for the sake of completeness. For simplicity, assume that  $t = MK/N$  is an integer (if not, a memory-sharing argument is used to multiplex between points for which this parameter is an integer [7]). Each file  $W_i$  is partitioned into segments<sup>2</sup>  $\{W_i^T : T \subseteq [K], |T| = t\}$  and each user  $k \in [K]$  caches all and only the segments  $W_i^T$  for all the subsets  $T$  such that  $T \ni k$ . It is easy to check that the cache of each user must have size

$$N \frac{F}{\binom{K}{t}} \binom{K-1}{t-1} = MF. \quad (1)$$

In the delivery phase, given a demand vector  $\mathbf{d} \in [N]^K$ , the server computes the codeword  $X$  obtained from the concatenation of blocks  $X_S$  for all  $S \subseteq [K], |S| = t+1$ . Each such block is given by

$$X_S = \bigoplus_{k \in S} W_{d_k}^{S \setminus \{k\}}, \quad (2)$$

where we notice that for any  $S$  of size  $t+1$  and  $k \in S$ , the set  $S \setminus \{k\}$  is a subset of size  $t$ , such that  $W_{d_k}^{S \setminus \{k\}}$  are effectively segments of the file desired by user  $k$  and cached at all users  $j \in S$ ,  $j \neq k$ . The multicast codeword defined in (2) corresponds to the original scheme proposed in [7]. A slight modification of this scheme yields given in [9] a better delivery rate when  $K < N$  and therefore some users necessarily request the same file. We hasten to say that all the results in this paper extend immediately to this improved scheme. The two delivery schemes for the worst-case demand coincide when  $K \geq N$ , since the worst case demand (i.e., the demand configuration that requires the longest multicast codeword) contains all distinct demands. The overall transmission length is given by

$$\mathcal{L}(X) = \frac{F}{\binom{K}{t}} \binom{K}{t+1} = \frac{FK(1-\mu)}{1+K\mu}, \quad (3)$$

where  $\mu = M/N$  is the fractional cache memory.

In our scheme,  $X$  is divided into  $L$  blocks of equal size, for some integer  $L \leq N_E$  and *Maximum Distance Separable* (MDS) coding is applied to append  $N_E - L$  parity blocks. Each

<sup>2</sup>For an integer  $n$  we let  $[n] = \{1, 2, \dots, n\}$ .

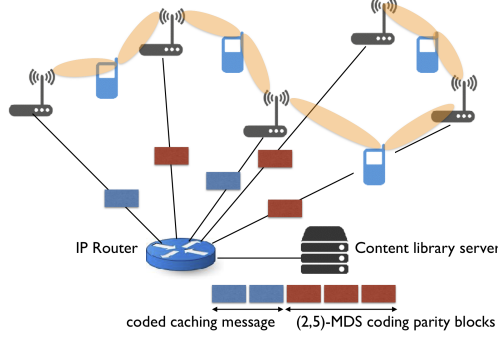


Fig. 1: A conceptual example of the proposed system with  $N_E = 5$  and  $L = 2$ . User nodes make use of their beamforming antenna array to decode two out of five EN transmissions, by treating the others as noise.

MDS-coded block is treated as a symbol over a large finite field, with length in bits given by  $\frac{1}{L}\mathcal{L}(X)$ . The resulting  $N_E$  MDS-coded blocks are sent to the  $N_E$  ENs, such that each EN is associated to a distinct MDS-coded block. Eventually, the blocks are transmitted through an appropriate physical-layer (PHY) coded modulation scheme and sent in parallel, on the same time-frequency slot, from the different ENs.

The users make use of their antenna array to detect and decode the PHY codewords of  $L$  ENs. Thanks to MDS coding, whenever a user  $k$  is able to decode  $L$  ENs messages, then it can reconstruct the whole multicast codeword  $X$ . In fact, the MDS condition is that the information message  $X$  can be reconstructed from any  $L$  out of  $N_E$  MDS-coded blocks. At this point, user  $k$  can decode the desired file  $d_k$  from  $X$  and its cache content, as detailed in [7]. Fig. 1 shows an example with  $N_E = 5$  and  $L = 2$ , where all users that can decode 2 data streams from two distinct ENs can retrieve their requested file.

The delivery latency, i.e., the time necessary to deliver all requests, is given by

$$D = \frac{1}{LR} \times \frac{F}{w} \times \frac{K(1-\mu)}{1+K\mu}, \quad (4)$$

where  $w$  is the bandwidth of the wireless channel and  $R$  is the PHY rate, also referred to as *spectral efficiency*, expressed in bit/s/Hz. Notice that  $D$  in (4) is given by the product of three factors:  $F/w$  depends on the file size and the system bandwidth (baudrate), and is fixed by the system design. The term  $\frac{K(1-\mu)}{1+K\mu}$  is the coded caching gain as in [7]. Finally,  $1/(LR)$  is the combined effect of MDS “macro-diversity order” and the PHY coding rate. *Our main system design goal consists of determining  $L$  such that the product  $LR$  is maximized (i.e., the delivery*

*latency is minimized) for a given target per-user outage probability.*

From the PHY viewpoint, the goal for each user is to successfully decode the  $L$  strongest ENs. Assuming that the PHY codewords are long enough such that the small-scale Rayleigh fading behaves as a stationary and ergodic process over the time-frequency slot spanned by a PHY codeword, we denote by  $C_{k,\ell}(\Phi)$  the achievable ergodic rate that user  $k$  can successfully decode *with high probability* (w.h.p.) from EN  $\ell$  for a given decoding strategy (to be detailed later) and a given geometry  $\Phi$ , i.e., a given placement of the ENs relative to user  $k$ . Without loss of generality, we can sort these achievable rates such that  $C_{k,1}(\Phi), \dots, C_{k,L}(\Phi)$  are the largest rates over all the NEs. It follows that user  $k$  can obtain its requested file if

$$C_k^{(L)}(\Phi) = \min\{C_{k,\ell}(\Phi) : \ell \in [L]\} > R, \quad (5)$$

For a random geometry  $\Phi$ , we can define the user outage probability as

$$P_{\text{out},k}(R) = \mathbb{P}(\min_{\ell \in [L]} C_{k,\ell}(\Phi) \leq R), \quad (6)$$

given by the Cumulative Distribution Function (CDF) of  $\min_{\ell \in [L]} C_{k,\ell}(\Phi)$ .

### III. SYSTEM PERFORMANCE ANALYSIS

We assume that ENs are randomly located on the two-dimensional plane and are distributed according to a two-dimensional homogeneous Poisson Point Process (PPP) of density  $\lambda$ . The ensemble of the locations of the ENs is denoted by  $\Phi$ . The propagation is characterized by small-scale Rayleigh fading that remains constant on time-frequency coherence blocks of  $n$  symbols (block fading model) and evolves according to a stationary ergodic process from block to block. Each receiving user acquires the downlink (DL) channel state information at the receiver (CSIR) from its surrounding ENs (e.g., through common DL pilots periodically broadcasted by the ENs). For simplicity, we do not consider CSIR error and pilot overhead in the present analysis. However, broadcasting downlink pilots, or “beacon” signals, from the base stations/access points is common practice of any current cellular system and WiFi network, so that the same type of overhead and (small) performance degradation incurred by any standard technology is to be expected in our system.

Given the symmetry of the problem, without loss of generality we can consider the performance of the typical user indexed by  $k$  and located at the origin. We sort the ENs according to their

distance from user  $k$  in non-decreasing order, and let  $j \in [N_E]$  be the index of the  $j$ -th closest EN to user  $k$ . The space-time signal received by user  $k$  is given by

$$\mathbf{Y}_k = \sum_{j=1}^{N_E} \sqrt{\beta r_{k,j}^{-\eta}} \mathbf{h}_{k,j} \mathbf{x}_j + \mathbf{N}_k \quad (7)$$

where  $\mathbf{Y}_k \in \mathbb{C}^{n_r \times n}$  with  $n$  being the size of the fading blocks in symbols,  $\mathbf{h}_{k,j} \in \mathbb{C}^{n_r \times 1}$  is the channel vector containing the small-scale fading coefficients from EN  $j$  to the array of user  $k$ ,  $\mathbf{x}_j \in \mathbb{C}^{1 \times n}$  is the coded-modulation block of symbol sent by EN  $j$ ,  $r_{k,j}$  is the distance between EN  $j$  and user  $k$ ,  $\eta$  is the pathloss exponent, and  $\beta$  is the path loss intercept. The ENs transmit at a constant average power  $\frac{1}{n} \mathbb{E}[\mathbf{x}_j \mathbf{x}_j^H] = P$ . The noise samples in the matrix  $\mathbf{N}_k$  are independent and identically distributed (IID)  $\sim \mathcal{CN}(0, N_0)$ . According to the independent Rayleigh statistics,  $\mathbf{h}_{k,j}$  are IID across users and ENs and have IID components  $\sim \mathcal{CN}(0, 1)$ .

We introduce here the *Partial Zero-Forcing* (PZF) receiver strategy, proposed for our system. Let  $\mathbf{H}_k = [\mathbf{h}_{k,1}, \dots, \mathbf{h}_{k,N_E}]$  denote the  $n_r \times N_E$  matrix of the channel coefficients from the EN antennas to user  $k$  antenna array, and, for a subset  $\mathcal{B} \subseteq [N_E]$ , let  $\mathbf{H}_{k,\mathcal{B}}$  denote the submatrix formed by the columns with indices  $j \in \mathcal{B}$ . PZF consists of applying linear zero-forcing only with respect to the signals of the  $L$  nearest ENs, whereas the signals of the remaining ENs with indices  $j > L$  are treated as noise. Assuming  $n_r \geq L$ , the receive filtering matrix of user  $k$  is defined as the pseudo-inverse of the  $n_r \times L$  matrix  $\mathbf{H}_{k,1:L}$ . This is given by

$$\mathbf{H}_{k,1:L}^\dagger = \mathbf{H}_{k,1:L} (\mathbf{H}_{k,1:L}^H \mathbf{H}_{k,1:L})^{-1}. \quad (8)$$

Denoting by  $\mathbf{h}_{k,\ell}^\dagger$ ,  $1 \leq \ell \leq L$ , the  $\ell$ -th column of  $\mathbf{H}_{k,1:L}^\dagger$  and by  $\mathbf{q}_{k,\ell} = \mathbf{h}_{k,\ell}^\dagger / \|\mathbf{h}_{k,\ell}^\dagger\|$  the normalized receive filtering vector corresponding to the  $\ell$ -th stream, the filtered output is written as

$$\begin{aligned} \tilde{\mathbf{y}}_{k,\ell} &= \mathbf{q}_{k,\ell}^H \mathbf{Y}_k \\ &= \frac{(\mathbf{h}_{k,\ell}^\dagger)^H}{\|\mathbf{h}_{k,\ell}^\dagger\|} \mathbf{h}_{k,\ell} \sqrt{\beta r_{k,\ell}^{-\eta}} \mathbf{x}_\ell + \sum_{j=L+1}^{N_E} \frac{(\mathbf{h}_{k,\ell}^\dagger)^H}{\|\mathbf{h}_{k,\ell}^\dagger\|} \mathbf{h}_{k,j} \sqrt{\beta r_{k,\ell}^{-\eta}} \mathbf{x}_j + \tilde{\mathbf{z}}_k \end{aligned} \quad (9)$$

where  $\tilde{\mathbf{z}}_k$  is the filtered noise vector with IID components  $\sim \mathcal{CN}(0, N_0)$ .

In the rest of this paper, for the sake of analytical tractability, we focus on the case of an infinitely extended network (i.e.,  $N_E \rightarrow \infty$ ) and high-SNR interference limited performance (i.e.,  $N_0 \rightarrow 0$ ). As a result, the system becomes “scale-free”, that is, the results of our analysis are invariant to any non-zero scaling factor of the physical distances  $r_{k,\ell}$  appearing in (9).



The Signal-to-Interference Ratio (SIR) at user  $k$  receiver is given by

$$\text{SIR}_{k,\ell} = \frac{r_{k,\ell}^{-\eta} \|\mathbf{h}_{k,\ell}^\dagger\|^{-2}}{\sum_{j=L+1}^{\infty} r_{k,j}^{-\eta} |\tilde{h}_{k,j}|^2}. \quad (10)$$

Since  $\mathbf{q}_{k,l}$  is a unit vector that is independent of  $\{\mathbf{h}_{k,j} : j = L+1, L+2, \dots\}$ , it follows that  $\tilde{h}_{k,j} = \mathbf{q}_{k,l}^\dagger \mathbf{h}_{k,j} \sim \mathcal{CN}(0, 1), \forall j \geq L+1$ . Furthermore, a well-known property of the ZF linear detector is that in the case of Gaussian IID channel vectors the useful signal coefficient  $\|\mathbf{h}_{k,l}^\dagger\|^{-2} = \mathcal{X}_{2(n_r-L+1)}$  is Chi-squared distributed with  $2(n_r - L + 1)$  degrees of freedom [23] and mean  $\mathbb{E}[\mathcal{X}_{2(n_r-L+1)}] = n_r - L + 1$ . The the ergodic achievable rate with Gaussian inputs and treating interference as noise for the transmission of the  $\ell$ -th closest EN at user  $k$  is given by

$$C_{k,\ell}(\Phi) = \mathbb{E} \left[ \log \left( 1 + \frac{r_{k,\ell}^{-\eta} \mathcal{X}_{2(n_r-L+1)}}{\sum_{j=L+1}^{\infty} r_{k,j}^{-\eta} |\tilde{h}_{k,j}|^2} \right) \middle| \Phi \right], \quad (11)$$

where the random variables  $\mathcal{X}_{2(n_r-L+1)}$  and  $|\tilde{h}_{k,j}|^2 : j > L$  are mutually independent, and the conditioning with respect to the geometry  $\Phi$  determines the distances  $r_{k,\ell}$  and  $r_{k,j} : j > L$ . In order to obtain analytically tractable expressions, we first apply Jensen's inequality with respect to the interference fading coefficients  $|\tilde{h}_{k,j}|^2, j \geq L+1$ . Using  $\mathbb{E}[|\tilde{h}_{k,j}|^2] = 1$  and the convexity of the function  $f(x) = \log(1 + a/x)$  for  $a > 0$  and  $x > 0$ , we obtain the achievable rate lower bound

$$C_{k,\ell}(\Phi) = \mathbb{E} \left[ \log \left( 1 + \rho_{k,\ell} \mathcal{X}_{2(n_r-L+1)} \right) \middle| \Phi \right]. \quad (12)$$

where we define the *local-average SIR*

$$\rho_{k,\ell} = \frac{r_{k,\ell}}{\sum_{j=L+1}^{\infty} r_{k,j}^{-\eta}}, \quad 1 \leq \ell \leq L. \quad (13)$$

that captures the network geometry. Next, we would like to eliminate the dependency on the distances  $r_{k,j}$  with  $j \geq L+1$ . To this purpose, we replace the conditioning with respect to  $\Phi$  by the conditioning with respect to only  $r_{k,\ell}$  and  $r_{k,L}$ , i.e., the  $\ell$ -th and the  $L$ -th shortest distances from the origin. Furthermore, letting  $I = \sum_{j=L+1}^{\infty} r_{k,j}^{-\eta}$  and noticing that  $r_{k,j}$  for  $j \geq L+1$  depends on PPP points outside the disk of radius  $r_{k,L}$  around user  $k$  while  $r_{k,\ell}$  depend on PPP points inside the disk, we have that [24]  $\mathbb{E}[I | r_{k,L}, r_{k,\ell}] = \mathbb{E}[I | r_{k,L}]$ . By applying this approximation and Jensen's inequality in (12), we obtain

$$C_{k,\ell}(\Phi) \gtrsim \mathbb{E} \left[ \log \left( 1 + \frac{r_{k,\ell}^{-\eta} \mathcal{X}_{2(n_r-L+1)}}{\sum_{j=L+1}^{\infty} r_{k,j}^{-\eta}} \right) \middle| r_{k,L}, r_{k,\ell} \right] \quad (14)$$

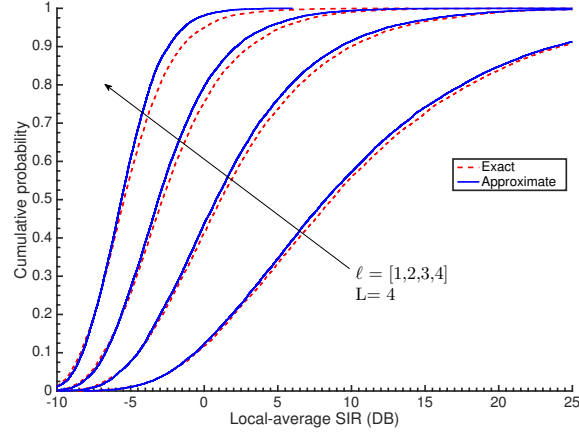


Fig. 2: CDFs of the exact and approximate local-average SIRs  $\rho_{k,\ell}$  and  $\tilde{\rho}_{k,\ell}$  with  $n_r = 8$ .

$$\geq \mathbb{E} \left[ \log \left( 1 + \frac{r_{k,\ell}^{-\eta} \mathcal{X}_{2(n_r-L+1)}}{\mathbb{E}[I | r_{k,L}]} \right) \middle| r_{k,L}, r_{k,\ell} \right]. \quad (15)$$

In order to calculate the conditional average interference term in (15), we apply Campbell theorem [24, Theorem 4.1] and, for  $\eta > 2$ , we obtain

$$\mathbb{E}[I | r_{k,L}] = \frac{2\pi\lambda}{\eta - 2} r_{k,L}^{2-\eta}. \quad (16)$$

Plugging (16) in (15), we obtain the quasi-lower bound<sup>3</sup> on the ergodic achievable rate in the form

$$C_{k,\ell}^{\text{qlb}}(\Phi) = \mathbb{E} \left[ \log \left( 1 + \tilde{\rho}_{k,\ell} \mathcal{X}_{2(n_r-L+1)} \right) \middle| \Phi \right]. \quad (17)$$

where we define the approximated conditional local-average SIR as

$$\tilde{\rho}_{k,\ell} = \frac{r_{k,L}^{\eta-2}}{r_{k,\ell}^{\eta}} \frac{\eta - 2}{2\pi\lambda} \quad 1 \leq \ell \leq L. \quad (18)$$

Notice that  $\tilde{\rho}_{k,\ell}$  is related to  $\rho_{k,\ell}$  defined in (13) by replacing the denominator  $I$  of (13) with its conditional expectation given in (16). This approach yields analytically tractable expressions and is expected to provide a very accurate approximation of the actual achievable ergodic rate for fixed geometry  $\Phi$  because the interference term  $I$  contains the cumulative effect of many “far” ENs, such that it is expected that a sort of self-averaging effect kicks in.

Fig. 2 compares the CDF of the local average SIR  $\tilde{\rho}_{k,\ell}$  obtained via approximation in (18) against its exact form  $\rho_{k,\ell}$  in (13). All the curves are obtained via Monte-Carlo simulations by

<sup>3</sup>This is referred to as quasi-lower bound because of the approximation in (14).

setting the EN density  $\lambda = 8 \text{ ENs/km}^2$  (which amounts to on average one EN in a circular cell of radius 200 m), the pathloss exponent  $\eta = 3.75$ . We assumed that the PZF is applied to cancel the  $L = 4$  nearest interferers at the receiving user equipped with antenna array size  $n_r = 8$ . As it can be seen from Fig. 2, the CDFs of  $\tilde{\rho}_{k,\ell}$  and  $\rho_{k,\ell}$  are very close for a wide range of SIR. Similar results have been observed for a great variety of system parameters.

### A. Main Results

We first present some distance distributions, which shall be useful in subsequent derivations. Given a homogeneous PPP  $\Phi$  of density of  $\lambda$ , let  $r_n$  denote the  $n$ -th shortest distance of points of  $\Phi$  from the origin. Then, the Probability Density Function (PDF) of  $r_n$  is given by [25]

$$f_{r_n}(v) = \frac{2(\pi\lambda)^n}{(n-1)!} v^{2n-1} e^{-\pi\lambda v^2}, \quad v \geq 0, \quad (19)$$

and the joint PDF of  $r_\ell$  and  $r_n$  with  $1 \leq \ell < n$  is given by [26]

$$f_{r_\ell, r_n}(u, v) = \frac{4(\pi\lambda)^n}{(n-\ell-1)!(\ell-1)!} (v^2 - u^2)^{n-\ell-1} v u^{2\ell-1} e^{-\pi\lambda v^2}, \quad u, v \geq 0. \quad (20)$$

Using these results, we next provide a closed-form accurate approximations for the outage probability and the average spectral efficiency in terms of the macro-diversity order  $L$ , the receive antenna array size  $n_r$ , the pathloss exponent  $\eta$ , and the delivery rate  $R$ .

#### 1) Outage probability

Based on the spatial distribution of the EN locations we can derive a distribution for the local-average SIR. Due to the difficulty of obtaining an exact closed-form for this distribution, we derive an approximate expressions based on the approach introduced in [27, 28]. First, the Laplace transform of the CDF of  $1/\tilde{\rho}_{k,\ell}$  is derived. Then, this is numerically inverted via Euler series expansion. Finally, the CDF can be obtained in the form of finite series yielding accurate results with only a few terms. Specifically, from [27], we obtain the sought approximated form for the CDF of  $1/\tilde{\rho}_{k,\ell}$  as

$$F_{\tilde{\rho}_{k,\ell}}(\gamma) \approx 1 - \gamma \frac{e^{A/2}}{2^B} \sum_{b=0}^B \binom{B}{b} \sum_{g=0}^{G+b} \frac{(-1)^g}{D_g} \text{Re} \left\{ \frac{\mathcal{L}_{1/\tilde{\rho}_{k,\ell}}(\tau)}{\tau} \right\}, \quad (21)$$

where

$$\tau = \frac{(A + i2\pi g)\gamma}{2}. \quad (22)$$

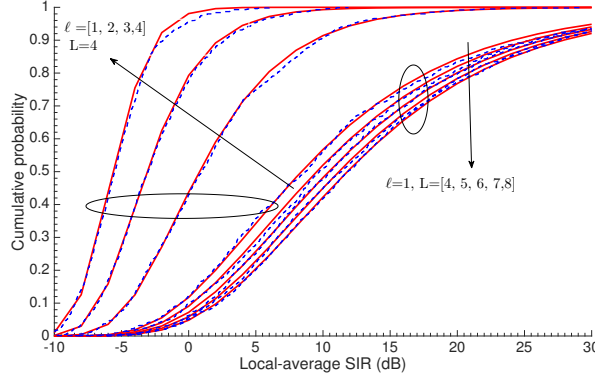


Fig. 3: CDF of the approximated local-average SIR ( $\tilde{\rho}_{k,\ell}$ ) with  $n_r = 8$ . Solid curves correspond to the analysis in (21) while the dashed curves are obtained via simulation.

The values  $D_0 = 2$  and  $D_g = 1$  for  $g > 0$  and  $A = 9.21$ ,  $B = 5$  and  $G = 8$  provide a satisfactory accuracy [29]. The Laplace transform of  $1/\tilde{\rho}_{k,\ell}$ , for  $s \in \mathbb{C}$ , is given by

$$\mathcal{L}_{1/\tilde{\rho}_{k,\ell}}(s) = \mathbb{E} [e^{-s/\tilde{\rho}_{k,\ell}}] \quad (23)$$

$$= \int_0^\infty dv \int_0^v e^{-s \frac{u^\eta}{v^{\eta-2}} \frac{2\pi\lambda}{\eta-2}} f_{r_{k,\ell}, r_{k,L}}(u, v) du \quad (24)$$

where  $f_{r_{k,\ell}, r_{k,L}}(u, v)$  is given by (20) with the replacement  $n \leftarrow L$ . Evaluating the integral in (24) separately for the two cases  $\ell < L$  and  $\ell = L$  yield the following compact expressions, proved in Appendix A.

**Case 1:** For  $\ell < L$

$$\mathcal{L}_{1/\tilde{\rho}_{k,\ell}}(s) = \sum_{n=0}^{L-\ell-1} \frac{(-1)^n \Gamma(L)}{(L-\ell-1)! (\ell-1)! (n+\ell)} \binom{L-\ell-1}{n} {}_2F_1\left(L, \eta'; \eta' + 1; \frac{-2s}{\eta-2}\right), \quad (25)$$

where  $\eta' = 2\frac{n+\ell}{\eta}$  and  ${}_2F_1(a, b; c; z)$  is the Gaussian hypergeometric function.

**Case 2:** For  $\ell = L$

$$\mathcal{L}_{1/\tilde{\rho}_{k,\ell}}(s) = \left( \frac{2s}{\eta-2} + 1 \right)^{-L}. \quad (26)$$

Fig. 3 illustrates the CDF of the approximated local-average SIR given in (21) with different sub-stream indices and different values of  $L$  with a receive antenna array size  $n_r = 8$ , EN density  $\lambda = 8$  ENs/km<sup>2</sup>, and  $\eta = 3.75$ . Monte Carlo simulation of the CDF is also reported for comparison, and shows that our analytical approximation is very accurate.

The expectation with respect to  $\mathcal{X}_{2(n_r-L+1)}$  in (17) can be calculated in closed form as

$$C_{k,\ell}^{\text{qlb}}(\tilde{\rho}_{k,\ell}) = \mathbb{E} [\log(1 + \tilde{\rho}_{k,\ell} \mathcal{X}_{n_r-L+1}) | \Phi]$$

$$= \mathcal{I}_{(n_r-L+1)}(\tilde{\rho}_{k,\ell}) \log(e), \quad (27)$$

where with a slight abuse of notation we use  $C_{k,\ell}^{\text{qlb}}(\tilde{\rho}_{k,\ell})$  instead of  $C_{k,\ell}^{\text{qlb}}(\Phi)$  since the dependency on the PPP points reduces to the single random variable  $\tilde{\rho}_{k,\ell}$ , and where we define the expression (see [30])

$$\begin{aligned} \mathcal{I}_M(\mu) &= \mathbb{E} [\log_e(1 + \mu \mathcal{X}_{2M})] \\ &= \Pi_M(-1/\mu) E_i(1, 1/\mu) + \sum_{m=1}^{M-1} \frac{1}{m} \Pi_m(1/\mu) \Pi_{M-m}(-1/\mu), \end{aligned} \quad (28)$$

with  $\Pi_n(x) = e^{-x} \sum_{i=0}^{n-1} \frac{x^i}{i!}$  and with the exponential integral function defined as  $E_i(n, x) = \int_1^\infty t^{-n} e^{-xt} dt$ . Due to the monotonicity of the log function,  $C_{k,\ell}^{\text{qlb}}(\tilde{\rho}_{k,\ell})$  is strictly monotonically increasing in  $\tilde{\rho}_{k,\ell}$ . Then, using  $C_{k,L}^{\text{qlb}}(\tilde{\rho}_{k,\ell})$  instead of  $C_k^{(L)}(\Phi)$  in the outage probability expression (6), we arrive at the desired quasi-upper bound to the outage probability in the form

$$\begin{aligned} P_k^{\text{out}}(R) &\lesssim \mathbb{P} \left( C_{k,L}^{\text{qlb}}(\tilde{\rho}_{k,L}) \leq R \right) \\ &= \mathbb{P} \left( \tilde{\rho}_{k,L} \leq \left( C_{k,L}^{\text{qlb}} \right)^{-1}(R) \right) \\ &= F_{\tilde{\rho}_{k,L}} \left( \left( C_{k,L}^{\text{qlb}} \right)^{-1}(R) \right), \end{aligned} \quad (29)$$

where the inverse function  $\left( C_{k,L}^{\text{qlb}} \right)^{-1}(\cdot)$  is easily obtained numerically from (27).

## 2) Average spectral efficiency

In order to appreciate the tradeoff between the macro-diversity order  $L$  and the achievable physical-layer transmission rate  $R$ , and to quickly see which value of  $L$  minimizes the delivery latency, we can consider the average spectral efficiency of a typical user when averaging is also with respect to the random locations of the ENs (i.e., with respect to  $\Phi$ ). We indicate by “overline” quantities averaged also with respect to the geometry. Then, we have

$$\overline{C}_{k,\ell} = \mathbb{E} \left[ \log \left( 1 + \frac{r_{k,\ell}^{-\eta} \mathcal{X}_{2(n_r-L+1)}}{\sum_{j=L+1}^{\infty} r_{k,j}^{-\eta}} \right) \right] \quad (30)$$

$$= \mathbb{E} \left[ \mathbb{E} \left[ \log \left( 1 + \frac{r_{k,\ell}^{-\eta} \mathcal{X}_{2(n_r-L+1)}}{\sum_{j=L+1}^{\infty} r_{k,j}^{-\eta}} \right) \middle| r_{k,L}, r_{k,\ell} \right] \right] \quad (31)$$

$$\geq \mathbb{E} \left[ \mathbb{E} \left[ \log \left( 1 + \tilde{\rho}_{k,\ell} \mathcal{X}_{2(n_r-L+1)} \right) \middle| r_{k,L}, r_{k,\ell} \right] \right] \quad (32)$$

$$= \mathbb{E} \left[ \log_2 \left( 1 + \tilde{\rho}_{k,\ell} \mathcal{X}_{2(n_r-L+1)} \right) \right] \quad (33)$$

**Remark 1:** Comparing (33) with (17) and using the law of iterated expectation, for which  $\mathbb{E} [\log (1 + \tilde{\rho}_{k,\ell} \mathcal{X}_{2(n_r-L+1)})] = \mathbb{E} [\mathbb{E} [\log (1 + \tilde{\rho}_{k,\ell} \mathcal{X}_{2(n_r-L+1)}) | \Phi]]$ , we have that the expectation of our quasi-lower bound  $C_{k,\ell}^{\text{qlb}}(\Phi)$  on the ergodic mutual information for a given geometry  $\Phi$  yields a true lower bound  $\bar{C}_{k,\ell}^{\text{lb}}$  on the average (w.r.t. the random geometry) ergodic mutual information.  $\diamond$

At this point, it is convenient to define

$$\widetilde{\text{SIR}}_{k,\ell} = \tilde{\rho}_{k,\ell} \mathcal{X}_{2(n_r-L+1)}, \quad (34)$$

as the ‘‘SIR’’ quantity appearing in (33) and evaluate the expectation by following the approach of [31]. We can write

$$\bar{C}_{k,\ell}^{\text{lb}} = \int_0^\infty \log_2(1 + \gamma) dF_{\widetilde{\text{SIR}}_{k,\ell}}(\gamma) \quad (35)$$

$$= \int_0^\infty (1 - F_{\widetilde{\text{SIR}}_{k,\ell}}(2^\gamma - 1)) d\gamma. \quad (36)$$

Notice that, for fixed  $\tilde{\rho}_{k,\ell}$ ,  $\widetilde{\text{SIR}}_{k,\ell}$  is chi-squared distributed (up to a scaling factor). Hence, its conditional CDF is given by

$$F_{\widetilde{\text{SIR}}_{k,\ell}|\tilde{\rho}_{k,\ell}}(\gamma) = 1 - \frac{\Gamma(n_r - L + 1, \gamma/\tilde{\rho}_{k,\ell})}{\Gamma(n_r - L + 1)}. \quad (37)$$

Where  $\Gamma(a, x) = \int_x^\infty t^{a-1} e^{-t} dt$  is the upper imcomplete gamma function. The unconditional CDF of  $\widetilde{\text{SIR}}_{k,\ell}$  is derived by expressing  $\tilde{\rho}_{k,\ell}$  in terms of  $r_{k,\ell}$  and  $r_{k,L}$  (cf. (18)) and using their joint PDF to average these variable out. The following expressions for  $F_{\widetilde{\text{SIR}}_{k,\ell}}(\cdot)$  are obtained by treating the two cases  $\ell < L$  and  $\ell = L$  separately (cf. Appendix B).

**Case 1:** For  $\ell < L$

$$\begin{aligned} F_{\widetilde{\text{SIR}}_{k,\ell}}(\gamma) = 1 - \sum_{m=0}^{n_r-L} \sum_{n=0}^{L-\ell-1} \frac{2(-1)^n}{m!(L-\ell-1)!(\ell-1)!\eta(\eta'+m)} \frac{\Gamma(m+L)}{n} \binom{L-\ell-1}{n} \\ \cdot \left(\frac{2\gamma}{\eta-2}\right)^m {}_2F_1\left(L+m, m+\eta'; m+\eta'+1; -\frac{2\gamma}{\eta-2}\right) \end{aligned} \quad (38)$$

**Case 2:** For  $\ell = L$

$$F_{\widetilde{\text{SIR}}_{k,\ell}}(\gamma) = 1 - \sum_{m=0}^{n_r-L} \frac{(m+L-1)!}{m!(L-1)!} \frac{(\frac{2\gamma}{\eta-2})^m}{(\frac{2\gamma}{\eta-2}+1)^{(m+L)}}. \quad (39)$$

Finally, by invoking (38) and (39) in (36) and evaluating the integrals, the lower bound of the average ergodic spectral efficiency corresponding to the  $\ell$ -th data stream can be expressed as follows (cf. Appendix C):

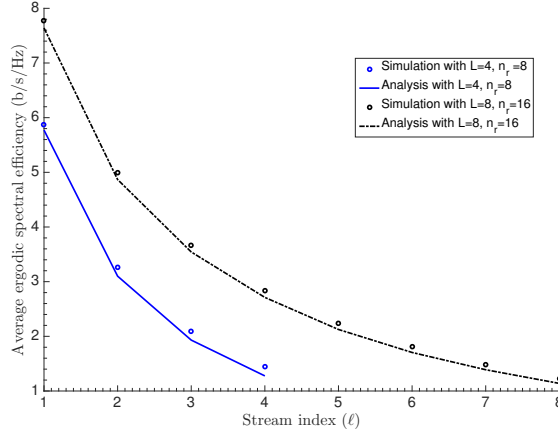


Fig. 4: Average ergodic spectral efficiency versus stream index.

**Case 1:** For  $\ell < L$

$$\begin{aligned} \bar{C}_{k,\ell}^{\text{lb}} = & \sum_{m=0}^{n_r-L} \sum_{n=0}^{L-\ell-1} \frac{2(-1)^n}{m!(L-\ell-1)!(\ell-1)!\eta} \binom{L-\ell-1}{n} \\ & \cdot G_{3,3}^{2,3} \left( \begin{matrix} -(m+1), -(m+L), -m-\eta' \\ -(m+1), -1, -(m+1+\eta') \end{matrix} \middle| \frac{2}{\eta-2} \right) \left( \frac{2}{\eta-2} \right)^{m+1} \log_2(e) \end{aligned} \quad (40)$$

where  $G_{m,n}^{p,q} \left( \begin{matrix} a_1, \dots, a_n, a_{n+1}, \dots, a_p \\ b_1, \dots, b_m, b_{m+1}, \dots, b_q \end{matrix} \middle| z \right)$  is Meijer-G function.

**Case 2:** For  $\ell = L$

$$\bar{C}_{k,L}^{\text{lb}} = \sum_{m=0}^{n_r-L} \frac{\log_2(e)}{m+L} {}_2F_1 \left( 1, L; m+L+1; 1 - \frac{2}{\eta-2} \right). \quad (41)$$

The tightness of this lower bounds is illustrated in Fig. 4, comparing  $\bar{C}_{k,L}^{\text{lb}}$  and  $\bar{C}_{k,L}$  for the settings:  $\lambda = 8 \text{ ENs/km}^2$  and  $\eta = 3.75$  with  $n_r = 8, L = 4$  and with  $n_r = 16, L = 8$ . Since eventually the spectral efficiency is defined by the worst-case data stream, we define the lower bound for minimum average ergodic spectral efficiency as follows

$$\bar{C}_{k,\text{PZF}}^{\text{lb}} = \bar{C}_{k,L}^{\text{lb}}. \quad (42)$$

**Remark 2: Operational significance of the average ergodic spectral efficiency.** Since each user must receive  $L$  data streams from  $L$  nearest ENs, assuming that the typical user is able to receive at common rate  $R = \bar{C}_{k,\text{PZF}}^{\text{lb}}$  bit.s/Hz, we can consider the value of  $L$  that maximizes the product  $L \times \bar{C}_{k,\text{PZF}}^{\text{lb}}$  and yields the minimum delivery time. This has an operational

significance if the average ergodic rate was indeed achievable. In turns, this depends on how quickly the geometry changes with respect to the duration of a codeword. We remark here that in classical stochastic geometry analysis it is customary to mix the time dynamics of the small-scale fading and of the random geometry. As a matter of fact, the small-scale fading “mixes” (i.e., it loses memory) on time intervals of the order of the inverse of the Doppler bandwidth, i.e., typically between 1 and 10 ms. In contrast, the geometry (distances between a user and the ENs) evolves according to much slower dynamics, and typically can be considered constant on intervals between 1 and 10 s for users moving at vehicular speeds, and even much larger for nomadic users. Hence, the operational meaning of the average ergodic rate computed here in terms of achievable rate is questionable, and this is precisely the reason for which we focused mainly on the outage probability, where outages are defined with respect to the random geometry. Nevertheless, the product  $L \times \bar{C}_{k,\text{PZF}}^{\text{lb}}$  captures (in an average sense) the tradeoff between  $L$  and  $R$ . For a desired value of this product, making the EN messages shorter by increasing  $L$  allows to reduce the transmission rate  $R$ , but the users are required to decode signals from more ENs, such that eventually the outage probability of the worst stream (the  $L$ -th stream) becomes too large.  $\diamond$

### 3) PZF with Successive Interference Cancellation

Previously we considered the linear PZF detection strategy at the users for its analytical tractability. In this section we improve the PZF strategy by introducing successive interference cancellation (SIC). In PZF-SIC users decode their strongest EN signals in sequence. We let  $\Pi$  denote the set of permutations of  $[L]$ , and let  $\pi = \{\pi(1), \pi(2), \dots, \pi(L)\} \in \Pi$  denote the decoding order of a generic user  $k$ . Then, user  $k$  decodes  $\underline{\mathbf{x}}_{\pi(1)}$  first, by suppressing interference from the remaining  $L - 1$  ENs via ZF beamforming. Then, it subtracts the decoded version of  $\underline{\mathbf{x}}_{\pi(1)}$  from the received signal, and proceeds to the decoding of the next signal  $\underline{\mathbf{x}}_{\pi(2)}$  by suppressing interference from the remaining  $L - 2$  ENs via ZF beamforming. Notice that since we treat ergodic rates, each codeword must span a large number of fading states (i.e., channel matrices). Therefore, the decoding order cannot depend on the realization of the channel matrices, but only on their statistics, i.e., ultimately on the distance dependent path strengths. Assuming successful decoding and interference cancellation for the first  $\ell - 1$  SIC stages, the signal at the



input of the  $\ell$ -th decoding stage is given by

$$\mathbf{Y}_{k,\ell}^{\text{SIC}} = \sum_{j=\ell}^L \mathbf{h}_{k,\pi(j)} \sqrt{\beta r_{k,\pi(j)}^{-\eta}} \mathbf{x}_{\pi(j)} + \sum_{j=L+1}^{\infty} \mathbf{h}_{k,j} \sqrt{\beta r_{k,j}^{-\eta}} \mathbf{x}_j \quad \ell \leq L \quad (43)$$

Denoting by  $\mathbf{H}_{k,\pi(\ell:L)}$  the channel matrix restricted to ENs with indices  $\pi(\ell), \pi(\ell+1), \dots, \pi(L)$  and letting  $\mathbf{H}_{k,\pi(\ell:L)}^\dagger$  be the corresponding pseudo-inverse, the ZF beamforming vector for the  $\ell$ -th SIC stage is given by the first column of pseudo-inverse, denoted by  $[\mathbf{H}_{k,\pi(\ell:L)}^\dagger]_{:,1}$ , normalized to have unit norm. Letting  $\mathbf{v}_{k,\ell}$  denote such vector, the decoder input after ZF beamforming is given by

$$\tilde{\mathbf{y}}_{k,\ell}^{\text{SIC}} = \mathbf{v}_{k,\ell}^H \mathbf{Y}_{k,\ell}^{\text{SIC}} \quad (44)$$

$$= \mathbf{v}_{k,\ell}^H \mathbf{h}_{k,\pi(\ell)} \sqrt{\beta r_{k,\pi(\ell)}^{-\eta}} \mathbf{x}_{\pi(\ell)} + \sum_{j=L+1}^{\infty} \mathbf{v}_{k,\ell}^H \mathbf{h}_{k,j} \sqrt{\beta r_{k,j}^{-\eta}} \mathbf{x}_j. \quad (45)$$

Consequently, the  $\ell$ -th decoder SIR is given by

$$\text{SIR}_{k,\ell}^{\text{SIC}} = \frac{r_{k,\pi(\ell)}^{-\eta} \left| [\mathbf{H}_{k,\pi(\ell:L)}^\dagger]_{:,1} \right|^{-2}}{\sum_{j=L+1}^{\infty} r_{k,j}^{-\eta} |\tilde{h}_{k,j}|^2}. \quad (46)$$

Since  $\mathbf{v}_{k,\ell}$  is a unit vector that is independent of  $\{\mathbf{h}_{k,j} : j > L\}$ , as before it follows that  $\tilde{h}_{k,j} \sim \mathcal{CN}(0, 1), \forall j > L$ . Also, similarly as before, we have that the useful signal coefficient  $\left| [\mathbf{H}_{k,\pi(\ell:L)}^\dagger]_{:,1} \right|^{-2} = \mathcal{X}_{2(n_r - L + \ell)}$  is Chi-square distributed with  $2(n_r - L + \ell)$  degrees of freedom mean  $n_r - L + \ell$ . It follows that the ergodic spectral efficiency achievable at the  $\ell$ -th decoding stage is given by

$$C_{k,\ell}(\rho_{\pi(\ell)}) = \mathbb{E} \left[ \log \left( 1 + \frac{r_{k,\pi(\ell)}^{-\eta} \mathcal{X}_{2(n_r - L + \ell)}}{\sum_{j=L+1}^{\infty} r_{k,j}^{-\eta} |\tilde{h}_{k,j}|^2} \right) \middle| \Phi \right], \quad (47)$$

that, using Jensen's inequality, can be lower bounded by

$$C_{k,\ell}(\rho_{\pi(\ell)}) \geq \mathbb{E} \left[ \log \left( 1 + \rho_{k,\pi(\ell)} \mathcal{X}_{2(n_r - L + \ell)} \right) \middle| \Phi \right], \quad (48)$$

where  $\rho_{k,\ell}$  is defined in (13). Operating as before, we obtain the corresponding quasi-lower bound on the ergodic spectral efficiency at the  $\ell$ -th decoding stage as

$$C_{k,\ell}^{\text{qlb}}(\tilde{\rho}_{k,\pi(\ell)}) = \mathbb{E} \left[ \log \left( 1 + \tilde{\rho}_{k,\pi(\ell)} \mathcal{X}_{2(n_r - L + \ell)} \right) \middle| \Phi \right], \quad (49)$$

where  $\tilde{\rho}_{k,\ell}$  is defined in (18).

Next, we consider the outage probability of the PZF-SIC decoder. Notice that (48) is the ergodic achievable rate at the  $\ell$ -th stage assuming a genie-aided SIC decoder that has already

removed the codewords  $\underline{\mathbf{x}}_{\pi(1)}, \dots, \underline{\mathbf{x}}_{\pi(\ell-1)}$ . Then, we follow an argument similar to the one provided in [32], to show that for SIC, the error probability under genie-aided cancellation is the same as the actual error probability. It is important to notice that this statement holds only for the overall probability of error, and not for the individual probability of error of each decoding stage. We define the outage set  $\mathcal{A}$  as the set of all geometry configurations  $\Phi$  for which the PZF-SIC fails with very high probability (w.h.p). For any  $\Phi \in \mathcal{A}$  there exists  $1 \leq \ell^* \leq L$  such that

$$C_{k,\ell}(\rho_{k,\pi(\ell)}) > R, \quad \text{for } \ell = 1, \dots, \ell^* - 1, \quad \text{and} \quad C_{k,\ell^*}(\rho_{k,\pi(\ell^*)}) \leq R. \quad (50)$$

In other words,  $\ell^*$  is the index of the first stage (dependent on  $\Phi$ ) for which a decoding error occurs w.h.p.. Now, consider the set  $\mathcal{B}$  of geometry configurations  $\Phi$  such that  $\min_{\ell \in [L]} C_{k,\ell}(\rho_{k,\pi(\ell)}) \leq R$ . Since for any  $\Phi \in \mathcal{A}$  it is always true that  $\min_{\ell \in [L]} C_{k,\ell}(\rho_{k,\pi(\ell)}) \leq C_{k,\ell^*}(\rho_{k,\pi(\ell^*)}) \leq R$ , then  $\mathcal{A} \subseteq \mathcal{B}$ . On the other hand, let  $\hat{\ell}$  denote the index achieving the minimum of  $\{C_{k,\ell}(\rho_{k,\pi(\ell)}) : \ell \in [L]\}$ . For any  $\Phi \in \mathcal{B}$  we have  $C_{k,\hat{\ell}}(\rho_{k,\pi(\hat{\ell})}) \leq R$ . Therefore, there must exist some  $\ell^* \leq \hat{\ell}$  for which the condition (50) is verified (in fact, it has to be some  $\ell^* \in [1 : \hat{\ell}]$  including  $\hat{\ell}$  itself). Hence, we have  $\mathcal{B} \subseteq \mathcal{A}$ . Thus, we conclude that  $\mathcal{A} = \mathcal{B}$ , and the outage probability of the PZF-SIC decoder is given by  $P_{\text{out},k}(R) = \mathbb{P}(\min_{\ell \in [L]} C_{k,\ell}(\rho_{k,\pi(\ell)}) \leq R)$ . Using the same argument made for PZF in the previous section, we replace  $C_{k,\ell}(\rho_{k,\pi(\ell)})$  with its quasi-lower bound approximation (49) and obtain a quasi-upper bound to the outage probability of the PZF-SIC as

$$P_{\text{out},k}(R) \lesssim \mathbb{P}\left(\min_{\ell} C_{k,\ell}^{\text{qlb}}(\tilde{\rho}_{k,\pi(\ell)}) \leq R\right). \quad (51)$$

A problem that remains to be addressed is how to choose the optimal decoding order  $\pi \in \Pi$  that minimizes the outage probability. It is immediate to verify from (49) that the functions  $C_{k,\ell}^{\text{qlb}}(\rho)$  for  $\rho \in \mathbb{R}_+$  are monotonically increasing and that, for any  $\rho \in \mathbb{R}_+$ , they satisfy the dominance condition

$$C_{k,1}^{\text{qlb}}(\rho) \leq C_{k,2}^{\text{qlb}}(\rho) \leq \dots \leq C_{k,L}^{\text{qlb}}(\rho), \quad (52)$$

due to the order of the chi-squared variable in (49) that increases with  $\ell$ . Then, we have the following result, proved in Appendix D:

**Theorem 1:** Let  $f_1(x), \dots, f_L(x)$  be a collection of monotonically non-decreasing functions on  $\mathbb{R}$  such that, for all  $x \in \mathbb{R}$ ,  $f_1(x) \leq f_2(x) \leq \dots \leq f_L(x)$ . Then, for any  $L$ -tuple of values

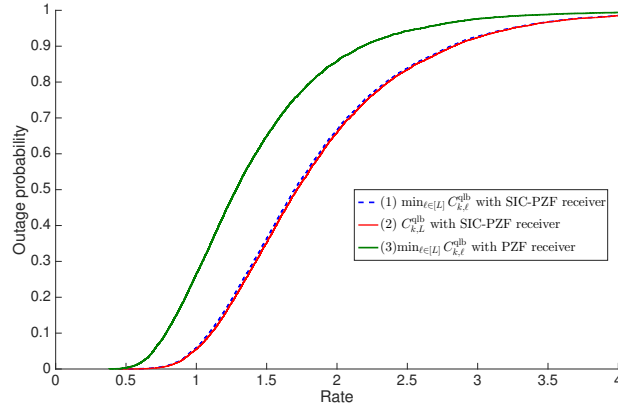


Fig. 5: Outage probability versus delivery rate with  $n_r = 8$ .

$$x_1 \geq \dots \geq x_L,$$

$$\max_{\pi \in \Pi} \min_{\ell \in [L]} f_\ell(x_{\pi(\ell)}) = \min_{\ell \in [L]} f_\ell(x_\ell), \quad (53)$$

i.e., the minimum of  $f_\ell(x_{\pi(\ell)})$  is maximized by the identity  $\pi(\ell) = \ell$  (although this may not be the unique solution).  $\square$

Notice that for any given realization of the geometry  $\Phi$ , the sequence  $\tilde{\rho}_{k,1}, \tilde{\rho}_{k,2}, \dots, \tilde{\rho}_{k,L}$  is monotonically decreasing. Therefore, the optimal PZF-SIC decoding order consists of decoding the EN signals in path strength order (strongest first,  $L$ -th strongest last, and treat all the others as noise).

In Fig. 5, the outage probability of the worst stream for cases with PZF and SIC-PZF are plotted. In PZF receiver, the last stream ( $L$ -th one) has the minimum ergodic spectral efficiency and defines the outage probability of PZF (as already written in (29)). However, for the PZF-SIC receiver the last stream is not necessarily the minimum for any realization of  $\Phi$ . The curves (1) and (2) in Fig. 5 show the CDFs  $\mathbb{P}\left(\min_{\ell \in [L]} C_{k,\ell}^{\text{qlb}}(\rho_{k,\ell}) \leq R\right)$  and  $\mathbb{P}\left(C_{k,L}^{\text{qlb}}(\rho_{k,L}) \leq R\right)$  for SIC-PZF. We notice that these two CDFs are almost identical. Therefore, for the sake of analytical tractability, we shall further relax our outage probability approximation for the PZF-SIC receiver to

$$P_{\text{out},k}(R) \lesssim \mathbb{P}\left(C_{k,L}^{\text{qlb}}(\tilde{\rho}_{k,L}) \leq R\right), \quad (54)$$

which can be obtained analytically by adapting the formulas of Section III-A1.

We conclude this section by providing a tight approximation of the average (over the geometry)

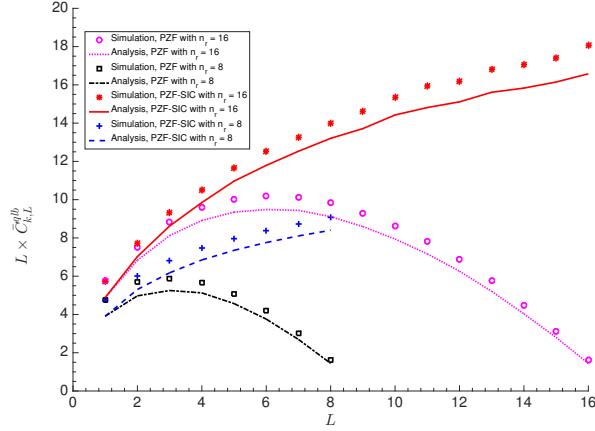


Fig. 6:  $L \times \bar{C}_{k,\text{PZF}}^{\text{qlb}}$  and  $L \times \bar{C}_{k,\text{PZF-SIC}}^{\text{qlb}}$  versus  $L \leq n_r$  for a typical user with  $n_r = 8, 16$ .

ergodic spectral efficiency of the PZF-SIC decoder. From what said before, it follows that

$$\begin{aligned} \bar{C}_{k,\text{PZF-SIC}}^{\text{qlb}} &= \mathbb{E} \left[ \min_{\ell \in [L]} C_{k,\ell}^{\text{qlb}}(\tilde{\rho}_{k,\ell}) \right] \\ &\approx \mathbb{E} \left[ C_{k,L}^{\text{qlb}}(\tilde{\rho}_{k,L}) \right], \end{aligned} \quad (55)$$

where the last line follows again by replacing the minimum with the  $L$  term. Using similar steps as done before for the PZF case with  $\ell = L$ , we obtain

$$\bar{C}_{k,\text{PZF-SIC}}^{\text{qlb}} = \sum_{m=0}^{n_r} \frac{\log_2(e)}{m+L} {}_2F_1 \left( 1, L; m+L+1; 1 - \frac{2}{\eta-2} \right). \quad (56)$$

#### IV. NUMERICAL RESULTS

In this section we provide some numerical results illustrating the behavior and the performance of the proposed content delivery wireless caching network. In order to generate the simulation results, the locations of ENs are distributed according to a homogeneous PPP restricted to a disk radius  $R_{\text{area}} = 3$  km with density  $\lambda = 8$  ENs/km<sup>2</sup>. The number of ENs is a Poisson random variable with mean  $\pi R_{\text{area}}^2 \lambda$  and the EN positions are generated independently with uniform probability over the disk. We considered realistic values of the pathloss exponent  $\eta = 3.75$  and the number of antennas  $n_r = 8, 16$  at the user receivers.

Fig. 6 compares, as a function of  $n_r$ ,  $L \times \bar{C}_{k,\text{PZF}}^{\text{qlb}}$  (cf. (42)) and  $L \times \bar{C}_{k,\text{PZF-SIC}}^{\text{qlb}}$  (cf. (56)) versus  $L$  for PZF and PZF-SIC receiver, which serves for the system designer a quick way to choose the best macro-diversity order  $L$  in order to minimize the delivery latency. With PZF,

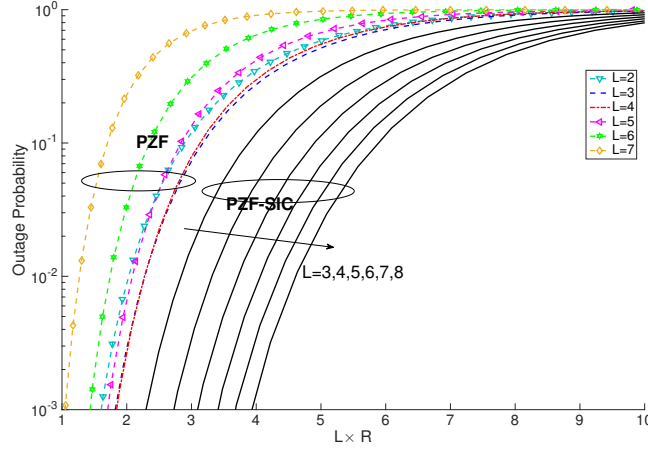


Fig. 7: Outage probability versus  $L \times R$  with  $n_r = 8$ .

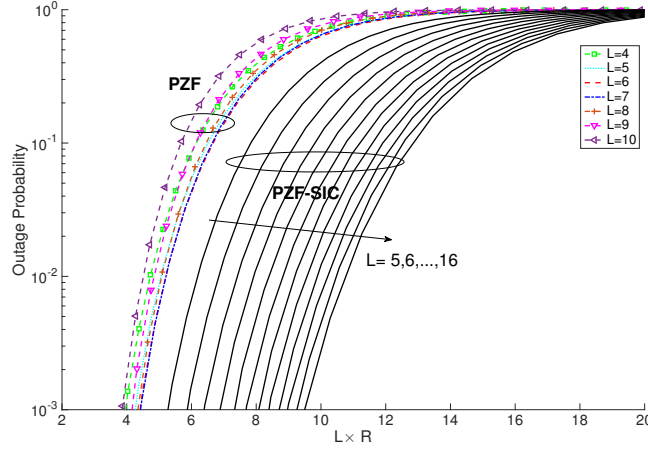


Fig. 8: Outage probability versus  $L \times R$  with  $n_r = 16$ .

the trade-off between PHY rate and macro-diversity order  $L$  is evident. In fact, the product  $L \times \bar{C}_{k,\text{PZF}}^{\text{lb}}$  increases for small  $L$ , reaches a maximum at  $L = 3$  for  $n_r = 8$  and at  $L = 6$  for  $n_r = 16$ , and then decreases, because the PHY rate at which the typical user can decode the  $L$ -th strongest EN decreases faster than the increase in  $L$ . In contrast, with PZF-SIC, the product  $L \times \bar{C}_{k,\text{PZF-SIC}}^{\text{qlb}}$  monotonically increases with  $L \in \{1, \dots, n_r\}$  showing that, at least for these system parameters, the best macro-diversity order is  $L = n_r$ .

Figs. 7 and 8 illustrate the outage probability versus  $L \times R$  with PZF and PZF-SIC receiver,  $n_r = 8$  and  $n_r = 16$ , respectively. For better exposition and simplicity of illustration, we only

bring the plots for some macro-diversity orders whose outage probability are the lowest. The missing macro diversity orders in these two figures have higher outage probability than the illustrated plots, so they do not play a role to find the best trade-off between the latency and the macro diversity order. The delivery latency varies with  $L \times R$  in an inverse manner and therefore moving to the right of these curves yields shorter delivery latency at higher outage probability (i.e., less and less users will be able to retrieve their requests, but those who can, receive it faster). In Fig. 7, by using PZF alone the macro-diversity order  $L = 3, 4$ , achieves better overall product  $L \times R$  and therefore lower delivery latency. In PZF-SIC, by increasing  $L$  the curves move to right side, indicating that for given target outage probability the delivery latency decreases by increasing the macro-diversity order  $L$ , confirming the behavior already observed for the average ergodic rate in Fig. 6. Similarly for  $n_r = 16$ , with PZF receiver macro-diversity  $L = 6, 7$  yield uniformly the best trade-off between latency and the outage probability while for PZF-SIC the best tradeoff is obtained by increasing  $L$ .

## V. CONCLUSION

In this paper, the coded caching paradigm is applied to a multipoint multicast system, somehow reminiscent of the current eMBMS for media broadcasting. In fact, the proposed system can be seen as a proposal to support on-demand multimedia delivery using the same principles of eMBMS, i.e., simultaneous transmission of a common multicast stream from multiple infrastructure nodes, referred to here as Edge Nodes (ENs). The key ingredients of our scheme are coded caching as proposed for the single bottleneck network, able to turn the individual demands into a single coded multicast stream in an information-theoretic optimal way, and MDS-coded multipoint multicast. The MDS code allows each user to retrieve the whole multicast message by decoding just  $L$  out of all possible EN transmissions. In this way, each user can select its “best”  $L$  ENs in a completely decentralized user-centric way. In our case, since the pathloss depends on distance, the best  $L$  ENs are the  $L$  closets ones.

Overall, the proposed system results in full spatial scalability, since the per-user throughput (resp., per-request delivery latency) does not vanish (resp., does not diverges to infinity) as the system coverage area grows without bound with constant user density, as long as also the density of the ENs is constant. We derived analytical expressions for the outage probability with respect

to the random network geometry and the average ergodic spectral efficiency for a typical user, where the averaging is also with respect to the network geometry. Our analysis shows that a rule of thumb to determine the optimal macro-diversity order  $L$  in the case of linear Partial Zero-Forcing (PZF) strategy at the users' receiver is to set  $L$  equal to half of the number of antennas  $n_r$  at the user receivers. In contrast, when PZF is augmented by Successive Interference Cancellation (SIC) in the order of the strongest EN (first) to the  $L$ -th strongest (last), letting  $L = n_r$  provides the best performance.

## APPENDIX A

### PROOF OF (25), (26)

**Case 1:** For  $\ell < L$

$$\mathcal{L}_{1/\tilde{\rho}_{k,\ell}}(s) = \int_0^\infty dv \int_0^v e^{-s \frac{u^\eta}{v^{\eta-2}} \frac{2\pi\lambda}{\eta-2}} f_{r_{k,\ell}, r_{k,L}}(u, v) du. \quad (57)$$

The joint PDF of  $f_{r_{k,\ell}, r_{k,L}}(u, v)$  is given by (20) with  $n \leftarrow L$ ,  $\ell \leftarrow \ell$ . By replacing the expression for the joint PDF, we have

$$\begin{aligned} \mathcal{L}_{1/\tilde{\rho}_{k,\ell}}(s) = \int_0^\infty dv \int_0^v e^{-s \frac{u^\eta}{v^{\eta-2}} \frac{2\pi\lambda}{\eta-2}} & \frac{4(\pi\lambda)^L}{(L-\ell-1)!(\ell-1)!} \\ & \cdot (v^2 - u^2)^{L-\ell-1} v u^{2\ell-1} e^{-\pi\lambda v^2} du, \end{aligned} \quad (58)$$

where after invoking the binomial expansion for  $(v^2 - u^2)^{L-\ell-1}$ , we obtain

$$\begin{aligned} \mathcal{L}_{1/\tilde{\rho}_{k,\ell}}(s) = \sum_{n=0}^{L-\ell-1} & \frac{4(\pi\lambda)^L}{(L-\ell-1)!(\ell-1)!} \binom{L-\ell-1}{n} (-1)^n \\ & \cdot \int_0^\infty v^{2(L-\ell-1-n)+1} e^{-\pi\lambda v^2} dv \int_0^v e^{-s \frac{2\pi\lambda}{\eta-2} \frac{u^\eta}{v^{\eta-2}}} u^{2\ell-1+2n} du. \end{aligned} \quad (59)$$

First, we apply a change of variable  $u^\eta \rightarrow x$  and then utilize [33, 3.351.1] to solve the inner integral. After simplification, we have

$$\mathcal{L}_{1/\tilde{\rho}_{k,\ell}}(s) = \sum_{n=0}^{L-\ell-1} \frac{4(\pi\lambda)^L}{(L-\ell-1)!(\ell-1)!} \binom{L-\ell-1}{n} (-1)^n \int_0^\infty v^{\nu+1} e^{-\pi\lambda v^2} \bar{\Gamma}\left(2\frac{n+\ell}{\eta}, s\alpha_1 v^2\right) dv, \quad (60)$$

where  $\nu = 2((L - \ell - 1 - n) + (\eta - 2)\frac{n+\ell}{\eta})$  and  $\alpha_1 = \frac{2\pi\lambda}{\eta-2}$ . Then, we invoke the change the variable  $v^2 \rightarrow x$  once more and then utilize the identity [33, 6.455.2] to obtain following result

$$\begin{aligned} \mathcal{L}_{1/\tilde{\rho}_{k,\ell}}(s) &= \sum_{n=0}^{L-\ell-1} \frac{(-1)^n \Gamma(L)}{(L-\ell-1)! (\ell-1)! (n+\ell)} \binom{L-\ell-1}{n} \\ &\quad \cdot (1 + \alpha_2 s)^{-L} {}_2F_1\left(1, L; \eta' + 1; \frac{\alpha_2 s}{1 + \alpha_2 s}\right) \end{aligned} \quad (61)$$

where  $\alpha_2 = \frac{2}{\eta-2}$ ,  $\eta' = 2\frac{n+\ell}{\eta}$ . Finally, by using the formula [33, 9.131.1] the Laplace transform can be rewritten as in (25).

**Case 2:** For  $\ell = L$

$$\mathcal{L}_{1/\tilde{\rho}_{k,L}}(s) = \int_0^\infty e^{-sv^2 \frac{2\pi\lambda}{\eta-2}} f_{r_{k,L}}(v) dv, \quad (62)$$

The marginal PDF  $f_{r_{k,L}}(v)$  is given by (19) with  $n \leftarrow L$ . After replacing the expression for the marginal PDF, we have

$$\mathcal{L}_{1/\tilde{\rho}_{k,L}}(s) = \int_0^\infty e^{-sv^2 \frac{2\pi\lambda}{\eta-2}} \frac{2(\pi\lambda)^L}{(L-1)!} v^{2L-1} e^{-\pi\lambda v^2} dv, \quad (63)$$

To solve this integral first we apply the variable change  $v^2 \rightarrow x$  and then use [33, 3.351.3], which gives (26).

## APPENDIX B

### PROOF OF (38) AND (39)

**Case 1:** For  $\ell < L$

$$F_{\widetilde{\text{SIR}}_{k,\ell}}(\gamma) = 1 - \int_0^\infty \int_0^v (1 - F_{\widetilde{\text{SIR}}_{k,\ell}}(\gamma | r_{k,\ell}, r_{k,L})) f_{r_{k,\ell}, r_{k,L}}(u, v) du dv. \quad (64)$$

By direct substitution of the expression (37) into (64), we have

$$\begin{aligned} F_{\widetilde{\text{SIR}}_{k,\ell}}(\gamma) &= 1 - \int_0^\infty \int_0^v \frac{\Gamma\left(n_r - L + 1, \gamma \frac{2\pi\lambda}{\eta-2} \frac{u^\eta}{v^{\eta-2}}\right)}{\Gamma(n_r - L + 1)} \\ &\quad \cdot \frac{4(\pi\lambda)^L}{(L-\ell-1)! (\ell-1)!} (v^2 - u^2)^{L-\ell-1} v u^{2\ell-1} e^{-\pi\lambda v^2} du dv. \end{aligned} \quad (65)$$

Note that by using [33, 8.352.2] we can expand the incomplete gamma function and then we have

$$F_{\widetilde{\text{SIR}}_{k,\ell}}(\gamma) = 1 - \sum_{m=0}^{n_r-L} \frac{4(\pi\lambda)^L}{(L-\ell-1)! (\ell-1)! m!}$$



$$\cdot \int_0^\infty \int_0^v \left( \gamma \frac{2\pi\lambda}{\eta-2} \frac{u^\eta}{v^{\eta-2}} \right)^m e^{-\gamma \frac{2\pi\lambda}{\eta-2} \frac{u^\eta}{v^{\eta-2}}} (v^2 - u^2)^{L-\ell-1} v u^{2\ell-1} e^{-\pi\lambda v^2} du dv. \quad (66)$$

After expanding binomial, we have

$$F_{\widetilde{\text{SIR}}_{k,\ell}}(\gamma) = 1 - \sum_{n=0}^{L-\ell-1} \sum_{m=0}^{n_r-L} \frac{4(\pi\lambda)^L (-1)^n}{(L-\ell-1)! (\ell-1)! m!} \left( \gamma \frac{2\pi\lambda}{\eta-2} \right)^m \binom{L-\ell-1}{n} \cdot \int_0^\infty v^{-m(\eta-2)+2(L-\ell-1-n)+1} e^{-\pi\lambda v^2} \int_0^v e^{-\gamma \frac{2\pi\lambda}{\eta-2} \frac{u^\eta}{v^{\eta-2}}} u^{2n+2\ell-1+m\eta} du dv \quad (67)$$

To solve the inner integral first we change the variable  $u^\eta \rightarrow x$  and then use [33, 3.351],

$$F_{\widetilde{\text{SIR}}_{k,\ell}}(\gamma) = 1 - \sum_{n=0}^{L-\ell-1} \sum_{m=0}^{n_r-L} \frac{4(\pi\lambda)^L (-1)^n}{(L-\ell-1)! (\ell-1)! m!} \binom{L-\ell-1}{n} \left( \gamma \frac{2\pi\lambda}{\eta-2} \right)^{-\eta'} \cdot \int_0^\infty v^{\nu+1} \bar{\Gamma}(\eta' + m, \gamma\alpha_1 v^2) e^{-\pi\lambda v^2} dv, \quad (68)$$

where  $\nu = (\eta-2)\eta' + 2(L-\ell-1-n)$  and  $\alpha_2 = \frac{2}{\eta-2}$ ,  $\eta' = 2\frac{n+\ell}{\eta}$

In the next step to solve the remaining outer integral, first we change the variable  $v^2 \rightarrow x$  and then use [33, 6.455.2] to obtain following result

$$F_{\widetilde{\text{SIR}}_{k,\ell}}(\gamma) = 1 - \sum_{n=0}^{L-\ell-1} \sum_{m=0}^{n_r-L} \frac{2(-1)^n \Gamma(m+L)}{(L-\ell-1)! (\ell-1)! m! \eta (\eta' + m)} \binom{L-\ell-1}{n} \cdot \frac{(\alpha_2 \gamma)^m}{(\alpha_2 \gamma + 1)^{m+L}} {}_2F_1 \left( 1, L+m; \eta' + m + 1; \frac{\alpha_2 \gamma}{1 + \alpha_2 \gamma} \right).$$

where  $\alpha_2 = \frac{2}{\eta-2}$ . Finally, we use the formula [33, 9.131.1] to rewrite the preceding expression as (38).

**Case 2:** For  $\ell = L$

As previous case, the complement CDF of SIR can be written as follows

$$F_{\widetilde{\text{SIR}}_{k,L}}(\gamma) = 1 - \int_0^\infty \frac{\Gamma(n_r - L + 1, v^2 \gamma \frac{2\pi\lambda}{\eta-2})}{\Gamma(n_r - L + 1)} \frac{2(\pi\lambda)^L}{(L-1)!} v^{2L-1} e^{-\pi\lambda v^2} dv. \quad (69)$$

Note that by using [33, 8.352.2] we can expand the incomplete gamma function and then then the preceding integral can be written as follows

$$F_{\widetilde{\text{SIR}}_{k,L}}(\gamma) = 1 - \sum_{m=0}^{n_r-L} \frac{2(\pi\lambda)^L}{(L-1)! m!} (\gamma\alpha_1)^m \int_0^\infty v^{2m+2L-1} e^{-(\pi\lambda + \alpha_1 \gamma) v^2} dv, \quad (70)$$

where  $\alpha_1 = \frac{2\pi\lambda}{\eta-2}$ . After solving the integral by using [33, 3.351.3] and simplify the result, the final expression can be written as (39).

APPENDIX C  
PROOF OF (40) AND (41)

The average spectral efficiency can be computed by a integral which we provided in (36).

**Case 1:** For  $\ell < L$

$$\bar{C}_{k,\ell}^{\text{lb}} = \int_0^\infty 1 - F_{\widetilde{\text{SIR}}_{k,\ell}}(2^\gamma - 1) d\gamma \quad (71)$$

By substituting the complement CDF of SIR from (38) into the preceding expression, we have

$$\begin{aligned} \bar{C}_{k,\ell}^{\text{lb}} = & \sum_{m=0}^{n_r-L} \sum_{n=0}^{L-\ell-1} \frac{2(-1)^n}{m!(L-\ell-1)!(\ell-1)!\eta(\eta'+m)} \binom{L-\ell-1}{n} \\ & \cdot \int_0^\infty (\alpha_2(2^\gamma - 1))^m {}_2F_1(L+m, m+\eta'; m+\eta'+1; -(2^\gamma - 1)\alpha_2) d\gamma. \end{aligned} \quad (72)$$

By changing  $2^\gamma - 1 \rightarrow x$  and using of [33, 9.34.7], the hypergeometric function can be expressed in terms of the Meijer-G function as follows

$$\begin{aligned} \bar{C}_{k,\ell}^{\text{lb}} = & \sum_{m=0}^{n_r-L} \sum_{n=0}^{L-\ell-1} \frac{2(-1)^n}{m!(L-\ell-1)!(\ell-1)!\eta} \binom{L-\ell-1}{n} \log_2(e) \\ & \cdot \int_0^\infty (\alpha_2 x)^{m+1} (x+1)^{-1} G_{2,2}^{1,2} \left( \begin{matrix} -(m+L), -m-\eta' \\ -1, -(m+1+\eta') \end{matrix} \middle| \alpha_2 x \right) dx \end{aligned} \quad (73)$$

and the preceding integral has the explicit solution in [33, 7.811.5] and is provided the final expression in (40).

**Case 2:** For  $\ell = L$

$$\bar{C}_{k,L}^{\text{lb}} = \int_0^\infty F_{\widetilde{\text{SIR}}_{k,L}}^c(2^\gamma - 1) d\gamma \quad (74)$$

by changing varibale to  $2^\gamma \rightarrow e^\gamma$ , then the integral is rewritten as

$$\bar{C}_{k,L}^{\text{lb}} = \sum_{m=0}^{n_r-L} \frac{(m+L-1)! \log_2 e}{m!(L-1)!} \frac{1}{y^L} \int_0^\infty \frac{e^{-\gamma L} (1 - e^{-\gamma})^m}{(1 + \frac{1-y}{y} e^{-\gamma})^{m+L}} d\gamma \quad (75)$$

The integral can be solved by using of [33, 3.312.3]. The final expression for the integral is

$$\bar{C}_{k,L}^{\text{lb}} = \sum_{m=0}^{n_r-L} \frac{(m+L-1)!}{m!(L-1)!} \log_2(e) \frac{\Gamma(L)\Gamma(m+1)}{\Gamma(m+L+1)} {}_2F_1\left(1, L; m+L+1; 1 - \frac{2}{\eta-2}\right). \quad (76)$$

After simplification, the final expression for average spectral efficiency for the last sub-stream will be derived and be given by (41).

## APPENDIX D

### PROOF OF THEOREM 1

Consider the  $L \times L$  matrix  $\mathbf{T}$  with  $(i, j)$  elements  $T_{i,j} = f_i(x_j)$ ,  $i \in [L]$ ,  $j \in [L]$ . The elements  $T_{i,j}$  form a partially ordered set. By construction, two elements  $T_{i,j}$  and  $T_{i,j'}$  on the same row  $i$  are ordered such that  $T_{i,j} \geq T_{i,j'}$  for  $j \leq j'$ , and two elements  $T_{i,j}$  and  $T_{i',j}$  on the same column  $j$  are ordered such that  $T_{i,j} \geq T_{i',j}$  for  $i \geq i'$ .

Consider the Manhattan topology induced by the squared integer grid of the matrix indices (similar to the moves of the Rook on a chess board). Any two elements in the array are connected by a path formed by a horizontal move followed by a vertical move. A horizontal move to the left decreases the column index. A vertical move down increases the row index. Hence, the above inequalities imply that if two elements  $T_{i,j}$  and  $T_{i',j'}$  are connected by a path formed by a left horizontal move followed by a down vertical move (we write  $(i, j) \vdash (\leftarrow, \downarrow) \dashv (i', j')$ ), we can conclude that  $T_{i,j} \leq T_{i',j'}$ . In contrast, any move containing a right horizontal move or an up vertical move does not lead to a necessary ordering of the elements, since these moves go against the monotonicity of the elements in the same row and in the same column given above.

Consider any permutation  $\pi \in \Pi$ , represented as  $L \times L$  binary matrix  $\mathbf{P}_\pi$  with a single 1 in each row and column, where  $\mathbf{\Pi}_{\text{id}}$  is the identity matrix corresponding to the identity permutation  $\text{id}$ . We denote by  $\mathcal{S}_\pi$  the support of  $\mathbf{P}_\pi$ , i.e., the list of the positions of its “ones”, i.e.,  $\mathcal{S}_\pi = \{(i, j) : [\mathbf{P}_\pi]_{i,j} = 1\}$ . The set of values  $\{f_\ell(x_{\pi(\ell)}) : \ell \in [L]\}$  are obtained by retaining the elements of  $\mathbf{T}$  corresponding to the “ones” of  $\mathbf{P}_\pi$ . In particular,  $T_{\min, \pi} = \min\{T_{i,j} : (i, j) \in \mathcal{S}_\pi\}$  is the minimum corresponding to permutation  $\pi$  appearing in the right-hand side of (53). A transposition consists of exchanging two rows of  $\mathbf{\Pi}_\pi$ . Assume  $(i, j) \in \mathcal{S}_\pi$  and  $(i', j') \in \mathcal{S}_\pi$ , and consider the permutation  $\pi'$  obtained from  $\pi$  by transposition of rows  $i$  and  $i'$ . It follows that  $\mathcal{S}_{\pi'}$  contains the same elements of  $\mathcal{S}_\pi$  with the exception of  $(i, j), (i', j')$  which are replaced by  $(i, j'), (i', j)$ . The following statement is immediate (details are omitted for the sake of space limitation): consider  $\mathbf{P}_\pi$  and two positions  $(i, j)$  and  $(i', j')$  in its support  $\mathcal{S}_\pi$  and consider  $\mathbf{P}'_\pi$  obtained from  $\mathbf{P}_\pi$  by transposition of rows  $i$  and  $i'$ . If  $(i, j) \vdash (\leftarrow, \downarrow) \dashv (i', j')$ , then  $T_{\min, \pi'} \geq T_{\min, \pi}$ . We call such transposition a *minimum non-decreasing transposition*. Notice that any permutation  $\pi \neq \text{id}$  has at least a pair of positions  $(i, j)$  and  $(i', j')$  in  $\mathcal{S}_\pi$  such that  $(i, j) \vdash (\leftarrow, \downarrow) \dashv (i', j')$ . Hence, if  $\pi$  achieves the max in (53), then  $\pi'$  obtained by minimum non-decreasing transposition that

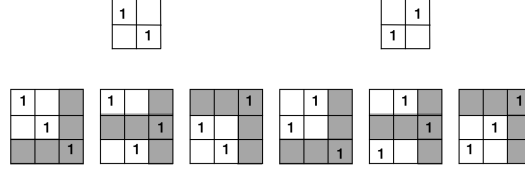


Fig. 9: Obtaining permutations of order  $L = 3$  from the permutations of order  $L = 2$  by adding a row and a column (shaded).

exchanges rows  $i$  and  $j$  also achieves the same max-min. It follows that the Theorem 1 is proved by showing that any  $\pi$  can be transformed into the identity permutation by a sequence of minimum non-decreasing transpositions.

The proof follows by induction. For  $L = 2$ ,  $\begin{bmatrix} 0 & 1 \\ 1 & 0 \end{bmatrix}$  can be turned into  $\begin{bmatrix} 1 & 0 \\ 0 & 1 \end{bmatrix}$  by transposing the rows, and obviously  $(1, 2) \vdash (\leftarrow, \downarrow) \dashv (2, 1)$ . Therefore, the statement holds for  $L = 2$ . Suppose that the statement is proved for  $L - 1$ . Notice that we can obtain the  $L!$  matrices of the order- $L$  permutations from the  $(L - 1)!$  matrices of the order- $(L - 1)$  permutations by inserting an additional row in all possible positions and column in last position with a single “one” at their intersection, to all the order- $(L - 1)$  matrices. Fig. 9 shows this augmentation process to go from  $L = 2$  to  $L = 3$ . For all order- $L$  matrices with the additional “one” in position  $(L, L)$  there is nothing to prove, since the  $(L - 1) \times (L - 1)$  upper left submatrix is an order- $(L - 1)$  permutation matrix, that we can transform into the identity by a sequence of minimum non-decreasing transpositions by the induction assumption. For all order- $L$  matrices with the additional “one” in position  $(i, L)$  for some  $1 \leq i \leq L - 1$ , we notice that the last row must contain a “one” in position  $(L, j)$  for  $j < L$ . Hence,  $(i, L) \vdash (\leftarrow, \downarrow) \dashv (L, j)$ , i.e., the transposition of rows  $L$  and  $i$  is minimum non-decreasing. After such transposition, we have a one in position  $(L, L)$  and the upper left  $(L - 1) \times (L - 1)$  upper left submatrix is an order- $(L - 1)$  permutation matrix, that can be transformed into the identity by a sequence of minimum non-decreasing transpositions. This concludes the proof. ■

## REFERENCES

- [1] N. Golrezaei, K. Shanmugam, A. Dimakis, A. Molisch, and G. Caire, “Femtocaching: Wireless video content delivery through distributed caching helpers,” in *INFOCOM, 2012 Proceedings IEEE*, March 2012, pp. 1107–1115.

- [2] N. Golrezaei, A. F. Molisch, A. G. Dimakis, and G. Caire, "Femtocaching and device-to-device collaboration: A new architecture for wireless video distribution," *IEEE Communications Magazine*, vol. 51, no. 4, pp. 142–149, 2013.
- [3] D. Liu, B. Chen, C. Yang, and A. F. Molisch, "Caching at the wireless edge: Design aspects, challenges, and future directions," *IEEE Communications Magazine*, vol. 54, no. 9, pp. 22–28, 2016.
- [4] G. Paschos, E. Bastug, I. Land, G. Caire, and M. Debbah, "Wireless caching: Technical misconceptions and business barriers," *IEEE Communications Magazine*, vol. 54, no. 8, pp. 16–22, 2016.
- [5] A. Sengupta, R. Tandon, and O. Simeone, "Cloud and cache-aided wireless networks: Fundamental latency trade-offs," *Wireless Communications (SPAWC)*, p. 1, 2016.
- [6] K. Poularakis and L. Tassiulas, "On the complexity of optimal content placement in hierarchical caching networks," *IEEE Transactions on Communications*, vol. 64, no. 5, pp. 2092–2103, 2016.
- [7] M. A. Maddah-Ali and U. Niesen, "Fundamental limits of caching," *IEEE Transactions on Information Theory*, vol. 60, no. 5, pp. 2856–2867, 2014.
- [8] —, "Decentralized coded caching attains order-optimal memory-rate tradeoff," *IEEE/ACM Transactions On Networking*, vol. 23, no. 4, pp. 1029–1040, 2015.
- [9] Q. Yu, M. A. Maddah-Ali, and A. S. Avestimehr, "The exact rate-memory tradeoff for caching with uncoded prefetching," in *Information Theory (ISIT), 2017 IEEE International Symposium on*. IEEE, 2017, pp. 1613–1617.
- [10] N. Naderializadeh, M. A. Maddah-Ali, and A. S. Avestimehr, "On the optimality of separation between caching and delivery in general cache networks," in *Proc. IEEE Int. Symp. Inform. Theory*, June 2017, pp. 1232–1236.
- [11] M. Ji, A. M. Tulino, J. Llorca, and G. Caire, "Caching in combination networks," in *Signals, Systems and Computers, 2015 49th Asilomar Conference on*. IEEE, 2015, pp. 1269–1273.
- [12] A. A. Zewail and A. Yener, "Coded caching for combination networks with cache-aided relays," in *Information Theory (ISIT), 2017 IEEE International Symposium on*. IEEE, 2017, pp. 2433–2437.
- [13] K. Wan, M. Ji, P. Piantanida, and D. Tuninetti, "Caching in combination networks: Novel multicast message generation and delivery by leveraging the network topology," *arXiv preprint arXiv:1710.06752*, 2017.
- [14] —, "Novel outer bounds and inner bounds with uncoded cache placement for combination networks with end-user-caches," *arXiv preprint arXiv:1701.06884*, 2017.
- [15] N. Mital, D. Gunduz, and C. Ling, "Coded caching in a multi-server system with random topology," *arXiv preprint arXiv:1712.00649*, 2017.
- [16] K.-H. Ngo, S. Yang, and M. Kobayashi, "Scalable content delivery with coded caching in multi-antenna fading channels," *arXiv preprint arXiv:1703.06538*, 2017.
- [17] O. Simeone, A. Maeder, M. Peng, O. Sahin, and W. Yu, "Cloud radio access network: Virtualizing wireless access for dense heterogeneous systems," *Journal of Communications and Networks*, vol. 18, no. 2, pp. 135–149, 2016.

- [18] A. Sanderovich, O. Somekh, H. V. Poor, and S. Shamai, "Uplink macro diversity of limited backhaul cellular network," *IEEE Transactions on Information Theory*, vol. 55, no. 8, pp. 3457–3478, Aug 2009.
- [19] S.-H. Park, O. Simeone, O. Sahin, and S. S. Shitz, "Fronthaul compression for cloud radio access networks: Signal processing advances inspired by network information theory," *IEEE Signal Processing Magazine*, vol. 31, no. 6, pp. 69–79, 2014.
- [20] M. Peng, S. Yan, K. Zhang, and C. Wang, "Fog-computing-based radio access networks: issues and challenges," *IEEE Network*, vol. 30, no. 4, pp. 46–53, 2016.
- [21] S.-H. Park, O. Simeone, O. Sahin, and S. Shamai, "Joint precoding and multivariate backhaul compression for the downlink of cloud radio access networks," *IEEE Transactions on Signal Processing*, vol. 61, no. 22, pp. 5646–5658, 2013.
- [22] R. Tandon and O. Simeone, "Cloud-aided wireless networks with edge caching: Fundamental latency trade-offs in fog radio access networks," in *Information Theory (ISIT), 2016 IEEE International Symposium on*. IEEE, 2016, pp. 2029–2033.
- [23] T. L. Marzetta, E. G. Larsson, H. Yang, and H. Q. Ngo, *Fundamentals of massive MIMO*. Cambridge, U. K.: Cambridge Univ. Press, 2016.
- [24] M. Haenggi, *Stochastic geometry for wireless networks*. Cambridge University Press, 2012.
- [25] —, "On distances in uniformly random networks," *IEEE Transactions on Information Theory*, vol. 51, no. 10, pp. 3584–3586, 20105.
- [26] F. J. Martin-Vega, F. J. Lopez-Martinez, G. Gomez, and M. C. Aguayo-Torres, "Multi-user coverage probability of uplink cellular systems: A stochastic geometry approach," in *Global Communications Conference (GLOBECOM), 2014 IEEE*. IEEE, 2014, pp. 3989–3994.
- [27] B. Błaszczyszyn and M. K. Karray, "Spatial distribution of the sinr in poisson cellular networks with sector antennas," *IEEE Transactions on Wireless Communications*, vol. 15, no. 1, pp. 581–593, 2016.
- [28] J. Abate and W. Whitt, "Numerical inversion of laplace transforms of probability distributions," *ORSA Journal on computing*, vol. 7, no. 1, pp. 36–43, 1995.
- [29] C. A. O'cinneide, "Euler summation for fourier series and laplace transform inversion," *Stochastic Models*, vol. 13, no. 2, pp. 315–337, 1997.
- [30] M.-S. Alouini and A. J. Goldsmith, "Capacity of rayleigh fading channels under different adaptive transmission and diversity-combining techniques," *IEEE Transactions on Vehicular Technology*, vol. 48, no. 4, pp. 1165–1181, 1999.
- [31] R. K. Mungara, D. Morales-Jiménez, and A. Lozano, "System-level performance of interference alignment," *IEEE Transactions on Wireless Communications*, vol. 14, no. 2, pp. 1060–1070, Feb. 2015.
- [32] B. Rimoldi and R. Urbanke, "A rate-splitting approach to the Gaussian multiple-access channel," *IEEE Transactions on Information Theory*, vol. 42, no. 2, pp. 364–375, 1996.
- [33] A. Jeffrey and D. Zwillinger, *Table of integrals, series, and products*. Academic press, 2007.